Spirolactone, an unprecedented antifungal *β*-lactone spiroketal macrolide from *Streptomyces iranensis*

Zhijie Yang,[a] Yijun Qiao,[a] Emil Strøbech,[a] Jens Preben Morth,[a] Grit Walther,[b,c] Tue Sparholt Jørgensen,[d] Gundela Peschel,[e] Miriam A. Rosenbaum,[e] Viola Previtali,[f] Mads Hartvig Clausen,[f] Marie Vestgaard Lukassen,[a] Charlotte H. Gotfredsen,[g] Oliver Kurzai,[b,c] Tilmann Weber,[d] Ling Ding[a,*]

[a] Department of Biotechnology and Biomedicine, Technical University of Denmark, Kgs Lyngby, Denmark.

[b] German National Reference Center for Invasive Fungal Infections, Leibniz Institute for Natural Product Research and Infection Biology – Hans Knöll Institute, Jena, Germany.

[c] Institute for Hygiene and Microbiology, University of Würzburg, Würzburg, Germany.

[d] The Novo Nordisk Foundation Center for Biosustainability, Technical University of Denmark, Kgs Lyngby, Denmark.

[e] BioPilot Plant, Leibniz Institute for Natural Product Research and Infection Biology – Hans Knöll Institute, Jena, Germany.

[f] Center for Nanomedicine and Theranostics, Department of Chemistry, Technical University of Denmark, Kemitorvet 207, DK-2800 Kgs. Lyngby, Denmark

[g] Department of Chemistry, Technical University of Denmark, Kemitorvet 207, DK-2800 Kgs. Lyngby, Denmark

*Corresponding author: Ling Ding lidi@dtu.dk

Abstract

Fungal infections pose a great threat to public health. There are only four classes of antifungals that have limitations due to high toxicity, drug-drug interactions, and emerging drug-resistance. *Streptomyces* spp. represent an important source of antimicrobial substances, notably including the antifungal agent amphotericin B. The rapamycin-producer *Streptomyces iranensis* displayed strong antifungal activities against *Aspergillus*. Revisiting its genome revealed several intriguing biosynthetic gene clusters, including one unparalleled Type I polyketide synthase, which codes for uncharacterized metabolites. The identification of a novel macrolide spirolactone (**1**) and its biosynthetic gene cluster was facilitated through CRISPR-based gene editing, HR-ESI-MS analysis, followed by fermentation and purification processes. Their structures and absolute configurations were confirmed by NMR, MS and X-ray crystallography. Spirolactone harbors an undescribed carbon skeleton with 13 chiral centers, featuring a rare *β*-lactone moiety, a [6,6]-spiroketal ring, and an unprecedented 7-oxo-octylmalonyl-CoA extender unit incorporated by a potential novel *Crotonyl*-CoA carboxylase/reductase. Spirolactone displayed profound antifungal effects against numerous fungal pathogens, e.g. the genus *Talaromyces* and several sections of *Aspergillus* including clinically relevant species such as *Aspergillus niger* and *A. tubingensis* (section Nigri), *A. terreus* (section Terrei) and the azol-resistant *A. calidoustus* (section Usti). Proteomics analysis revealed spirolactone potentially disrupted the integrity of fungal cell walls and induced the expression of stress-response proteins in *A. niger*. Spirolactone represents a new class of potential drug candidate to combat fungal infections.

Introduction

About 1.2 billion people worldwide are estimated to suffer from a fungal disease.[1] Invasive fungal diseases are particularly common among immunocompromised populations, such as patients with HIV/AIDS, chronic lung diseases, prior tuberculosis, cancer, diabetes, and patients receiving immunosuppressant treatment and invasive medical procedures.[2] Invasive fungal diseases are associated with unacceptably high mortality rates. The recent report suggested an annual incidence of 6.5 million invasive fungal infections and 3.8 million deaths.[3] Among those infections, *Aspergillus* has emerged as one of the most common causes of

56 infectious death in severely immunocompromised patients, with mortality rates up to 40% to
57 50% in patients with acute leukemia and recipients of hematopoietic stem cell transplantation.[1]
58 Furthermore, new risk cohorts are emerging, including patients with severe respiratory virus
59 infection such as influenza or COVID-19.[4] Currently, only four classes of systemic antifungal
60 medicines (azoles, echinocandins, pyrimidines, and polyenes) are used in clinical practice, and
61 only a limited number of candidates in the clinical development pipeline.[5-8] While existing
62 antifungal medications are effective in numerous instances, challenges persist due to side
63 effects and complications arising from drug-drug interactions.[9] Moreover, the emergence of
64 resistance has rendered some existing medications ineffective, and this is partly driven by the
65 inappropriate use of antifungals.[10] For example, agricultural use of azoles has been linked to
66 rising rates of azole-resistant *Aspergillus fumigatus* infections, with resistance rates of 15-20%
67 reported in parts of Europe and exceeding 80% in environmental samples from Asia.[10-12]
68 *Streptomyces* are producers of bioactive small molecules exhibiting a broad range of
69 structural and functional diversity called secondary or specialised metabolites (SMs).
70 Secondary metabolites are of great relevance to human health, offering pharmaceutical
71 properties such as antibacterial, antifungal, anticancer, and immunosuppressive activities.
72 Remarkably, all new drug approvals from 1981-2019 over 60% of the 1394 small molecule
73 drugs were either secondary metabolites (SMs) or derivatives thereof.[13-15] Nearly two-thirds of
74 antibiotics approved for clinical use originate from *Streptomyces*, and of Polyketides represent
75 a large and diverse group of *Streptomyces*-derived SMs, and many of them possess valuable
76 antifungal properties, among which nystatin and amphotericin B are two active polyenes used
77 clinically as first-line drugs to treat fungal infections. The first example is the antifungal drug
78 nystatin isolated from *Streptomyces noursei* in 1950 by Hazen and Brown.[16] Amphotericin B,
79 isolated from *Streptomyces nodosus* in 1955, remains a crucial component in the therapeutic
80 arsenal for combating invasive fungal diseases and leishmaniasis.[17] Recent studies revealed
81 that the mode of action of polyenes antibiotics involves acting as sterol "sponges" and
82 extracting ergosterol from the fungal membrane, causing cell death, in addition to the classical
83 model of pore formation in the fungal cell membrane.[18-20] Amphotericin B has been used to
84 treat mucormycosis, aspergillosis, blastomycosis, candidiasis, coccidioidomycosis, and
85 cryptococcosis. However, adverse effects for amphotericin B treatment are common, with

86 nephrotoxicity being the most serious.[21,22] There has been a continued interest in finding new
87 antifungal metabolites, such as turonicin A, hygrobafilomycin, iseolides, cyphomycin,
88 azalomycins, niphimycins, and resistomycin.[23-29] However, most exhibit non-selectivity and
89 display toxicity to human cells. Thus, it is of clinical importance to develop effective selective
90 antifungal drug candidates, with a new mode-of-action and low cytotoxicity.

91 Given the significant number of biosynthetic gene clusters (BGCs) present in *Streptomyces*,
92 a plethora of their metabolites remains undiscovered.[30] Access to modern analytical chemistry
93 techniques in combination with genetics and bioinformatics tools has enabled us to revisit the
94 "talented" microbes discovered decades ago.[31] *Streptomyces iranensis*, initially identified as a
95 rapamycin producer, was isolated from soil in Isfahan City, Iran.[32] Subsequent investigations
96 revealed its great capability to produce elaiophylin, azalomycins, nigericin, and other new
97 metabolites yet to be discovered.[33] In our recent research, we found that *S. iranensis* produced
98 pteridic acids H and F, which aid plants in coping with abiotic stress.[33] During our pipeline
99 search for antifungal polyketides, *S. iranensis* exhibited profound antifungal activity in co-
100 cultivation with *Aspergillus tubingensis* (*Supplementary information* Fig. 1), suggesting the
101 production of antifungal metabolites. Genome mining of *S. iranensis* indicated the presence of
102 an uncharacterized type-I modular polyketides BGC (*spl*) featuring sixteen modules, capturing
103 our particular interest. The product of this BGC namely spirolactone was carried out through
104 metabolomic analysis, large-scale fermentation and isolation. BGC (*spl*) was confirmed by
105 CRISPR-based gene mutation. The structures and absolute configurations of spirolactone was
106 elucidated using nuclear magnetic resonance (NMR), mass spectrometry (MS), and X-ray
107 crystallography. The striking structural features of spirolactone include a spiroketal ring, a rare
108 β-lactone moiety, and a distinctive polyketide synthetase (PKS) extender unit. Spirolactone
109 exhibits potent antifungal activity, potentially due to disrupting fungal cell wall integrity, as
110 suggested by label-free quantitative proteomics analysis. This study provides a paradigm for
111 mining novel molecules from extensive natural microorganisms, with the potential to lead to
112 the discovery of innovative antifungal agents to combat antimicrobial resistance.
113

114 **Results and Discussion**

115 **Genome mining of *S. iranensis*.** Due to the incompleteness of previously reported genomic

116 data, we performed whole-genome resequencing of *S. iranensis* using the combination of the
117 Oxford Nanopore Technologies MinION and Illumina MiSeq system. The high-resolution,
118 full-genome sequencing of *S. iranensis* reveals a linear chromosome spanning 12,213,033
119 nucleotides, featuring inverted terminal repeats comprising 156,145 nucleotides. The BGC
120 annotation of the acquired *S. iranensis* genome was carried out using antiSMASH version
121 7.0,[34] which resulted in the identification of a cryptic BGC (*spl* gene cluster) situated at the
122 terminal region of the linear chromosome (Fig. 1 and *Supplementary information* Fig. 2). The
123 gene cluster family (GCF) annotation of *spl* gene cluster showed it belongs to GCF_00315
124 and a total of 11 hits were detected (distance ≤ 900.0) in the BiG-FAM database
125 (*Supplementary information* Tab. 2).[35] The distinctive biosynthetic gene architecture of *spl*
126 gene cluster suggests its novelty as a modular Type-I PKS BGC, setting it apart from others
127 (*Supplementary information* Fig. 3). This finding spurred our interest in conducting a
128 thorough investigation of this individual BGC.

129 To locate the products of the potential *spl* gene cluster, we were elucidating the products
130 combining both genome editing and metabolomics. Initially, we constructed PKS knock-out
131 mutant (Δ*splA*) and crotonyl-CoA carboxylase/reductase-inactivated mutant (Δ*splH*) using the
132 CRISPR-Cas9 method and CRISPR base editing,[36] respectively (*Supplementary information* Fig.
133 4). Both mutants nearly abolished the antifungal activity against multiple *Aspergillus* strains.
134 Comparative metabolic profiling using LC-MS and LC-UV led to the identification of the
135 potential bioactive principle as a major compound **1** with *m/z* 881.4656 ($[M+Na]^+$) and other
136 derivatives, which were specifically abolished in both mutants (*Supplementary information*
137 Fig. 5). The complementation of pGM1190-based *splH* in mutant *S. iranensis*/Δ*splH* led to the
138 restoration of the production of **1** (*Supplementary information* Fig. 4).
139
140 **Characterization of spirolactone.** To obtain the products of the *spl* BGC, a 200 L
141 fermentation was carried out followed by a downstream processing using the open-column
142 chromatography on Amberchrom 161c resin, silica gel, Sephadex LH-20, and High-
143 Performance Liquid Chromatography (HPLC) to yield pure spirolactone (**1**). The structure was
144 elucidated by HR-ECI-MS, NMR spectroscopy, and X-ray crystallography.

Spirolactone (**1**) was obtained as a white solid and a molecular formula of $C_{47}H_{70}O_{14}$ by a sodium adduct ion (calcd *m/z* 881.4658 $[M+Na]^+$) was determined by HR-ESI-MS. It was assigned to the molecular formula on HR-ESI-MS combined with the NMR data. ^{1}H NMR spectrum revealed signals for six methyl groups H3-39 (δ 2.15), H3-41 (δ 0.94), H3-43 (δ 0.98), H3-44 (δ 0.93), H3-45 (δ 2.10), and OCH_3-8 (δ 3.37). Additionally, four olefinic protons were observed for H-2 (δ 6.19), H-3 (δ 7.91), H-4 (δ 6.47) and H-28 (δ 6.48). The coupling constant between H-2 and H-3 (*J* 15.4 Hz) confirmed a trans-orientation of a double bond. Besides the presence of several oxygen-bearing methines (H-6, H-8, H-10, H-14, H-16, and H-22), various other aliphatic proton signals were also observed (*Supplementary information* Fig. 6).

The ^{13}C NMR spectrum showed signals for several carbonyl groups, one carboxylic acid C-1 (δ 168.6), three keto- groups C-12 (δ 207.3), C-27 (δ 201.3) and C-38 (δ 209.6) and two ester groups C-40 (δ 161.8) and C-46 (δ 174.9), with C-40 from the β-lactone ring. Furthermore, signals were observed for six olefinic methines C-2 (δ 128.5), C-3 (δ 137.8), C-4 (δ 129.1), C-5 (δ 143.2), C-28 (δ 123.0), and C-29 (δ 156.4). Finally, signals for the methyl groups C-39 (δ 29.9), C-41 (δ 8.4), C-42 (δ 9.2), C-43 (δ 14.3), C-44 (δ 19.5), C-45 (δ 17.4) and the oxygenated methyl group 8-OMe (δ 59.6) connected to C-8 were also observed (*Supplementary information* Fig. 7). The chemical shift of C-18 (δ 101.0) indicated the presence of an acetal moiety. The ^{1}H and ^{13}C NMR data of **1** is shown in *Supplementary information*, Tab. 4.

COSY correlations further established six fragments including one saturated aliphatic chain. HMBC correlations (Fig. 2) further established a *β*-lactone moiety as HMBC correlations between H-6 and C-40 were observed. A further connection of this *β*-lactone to a polyene moiety was established by HMBC correlations between H-4 and C-6, as well as H-4 and C-40. A macrolactone bridge between H-10 and C-46 was established by HMBC correlation between them. The key HMBC correlation between H-13 and C-18 indicated the presence of an oxane ring. Moreover, H-16 and Me-43 showed HMBC correlations with C-18 (*Supplementary information* Fig. 8-13). Considering the double bond equivalence and the number of oxygen atoms inferred from HR-ESI-MS, a spiroketal structure was proposed. Finally, a planar structure with a novel carbon skeleton was proposed and named spirolactone. The complex structure exhibited no similarities to reported natural products. Meanwhile, the dispersion of the thirteen chiral centers made it challenging to elucidate the absolute configuration. Interestingly, the compound could form crystals from a dichloromethane/methanol solution.

177 One crystal was subjected to X-ray crystallography analysis, which successfully elucidated the
178 configurations (*Supplementary information* Fig. 14).

179 **Proposed biosynthesis of spirolactone.** The proposed *spl* gene cluster spanned 87.99 kb with
180 12 open reading frames (Fig. 1), including five core polyketide synthases (*splA*, *splC*, *splD*,
181 *splE*, and *splF*), a crotonyl-CoA carboxylase/reductase (*splH*), an *O*-methyltransferase (*splG*),
182 three cytochrome P450 (*splB*, *splK* and *splL*), and two hypothetical enzymes (*splI* and *splJ*)
183 (*Supplementary information* Tab. 3). The core PKS genes transcribed in the same direction
184 encoding genes within the *spl* BGC consist of one loading module and fifteen extender
185 modules, which are sequentially extended to form a linear polyketide chain by catalysis of
186 ketosynthase (KS) domain, acyltransferase (AT) domain, and acyl carrier protein (ACP), with
187 additional ketoreductase (KR), dehydratase (DH), and enoyl reductase (ER) domains. Based
188 on multiple sequence alignment, most KS domains keep the conserved catalytic sites comprised
189 of a cysteine (TA**C**SSS motif) as well as two histidines (EA**H**GTG and KSNIG**H**T motifs).[37]
190 Only the reactive cysteine in KS_1 was replaced by glutamine (*Supplementary information* Fig.
191 15), which was observed in the platensimycin/FabF (the type II FAS homology of KS)
192 complex.[38] The conserved fingerprint residues for extender unit selectivity, the GHSIG and
193 HAFH motifs are present in the nine AT domains (AT_1, AT_2, AT_5, AT_7, AT_8, AT_9, AT_{11}, AT_{12},
194 and AT_{14}) that are specifically binding to malonyl-CoA while GHSQG and YASH motifs are
195 present in the six AT domains (AT_3, AT_4, AT_6, AT_{10}, AT_{13}, and AT_{15}) that are specifically
196 binding to (*2S*)-methylmalonyl-CoA (*Supplementary information* Tab. 5 and Fig. 16).[37] AT_{16}
197 from module 15, which was thought to be accountable for loading distinct extender units,
198 exhibits an unusual IASH motif. KR domains have been previously classified into A1-, A2-,
199 B1-, and B2-types, which reduce ketones to their $_L$-hydroxy or $_D$-hydroxy counterparts.[39] We
200 determined that the KR_3, KR_4, and KR_{15} appear to belong to the B1-type: all have the
201 fingerprint LDD motif but the absence of a P residue in the catalytic region. KR_5 and KR_{12},
202 with the characteristic W residue but no LDD motif and H residue, were classified as A1-type
203 KRs (*Supplementary information* Fig. 17). The other KR domains couldn't be classified
204 according to the sequence, but they should be functional according to the structure of
205 spirolactone. Similarly, combined with structural information and conserved site analysis, the
206 five DH domains (DH_6, DH_7, DH_8, DH_9 and DH_{10}) were considered inactive during

207 spirolactone biosynthesis (*Supplementary information* Fig. 18). ER_{11} is classified as L-type due
208 to the presence of a tyrosine residue that donates a proton to the enol intermediate in L-type
209 ER, whereas ER_{13} and ER_{14} belong to D-type because it lacks tyrosine residue (*Supplementary*
210 *information* Fig. 19). The final release and cyclization of the linear product was probably
211 accomplished by TE domain in the last module, which contains an α/β-hydrolase catalytic core
212 and loop regions that form a substrate-binding lid.[40]

213 In the *spl* BGC, there are three cytochromes P450 enzymes (SplB, SplK, and SplL) with
214 conserved motifs of this family (*Supplementary information* Fig. 20).[41] The cytochrome P450
215 enzyme BonL from *Burkholderia gladioli* was previously identified to confer the C-22
216 carboxyl group in the biosynthesis of bongkrekic acid via sequential six-electron-oxidation.[42]
217 In addition, there are some cytochromes P450 enzymes that catalyze the carboxyl group
218 formation in microbial SMs, such as XiaM, PimG, AmphN, NysN, and FscP.[43-45] To identify
219 the cytochromes P450s responsible for carboxylation, we built the Hidden Markov model
220 (HMM) based on these sequences and the results showed that SplL exhibited the best match
221 with these known P450s with an E-value of 4e-117. In addition, bioinformatic analysis of XiaM
222 indicated that the P450s with carboxylation function harbor highly conserved segment
223 AGHET, which was also presented in SplK (*Supplementary information* Fig. 20). Therefore,
224 SplK and SplL, were considered putative candidates for catalyzing the two-step oxidation to
225 form carboxyl groups at positions C-1 and C-5 during spirolactone biosynthesis. SplB,
226 homologous cytochrome P450 monooxygenase CftA in clifednamide biosynthesis gene cluster
227 with 45.6% similarity,[46] was likely to accomplish the oxidation at C-27 in spirolactone. We
228 constructed mutant strains of *S. iranensis* inactivating the SplB, SplK and SplL enzymes
229 (denoted as Δ*splB*, Δ*splK*, and Δ*splL*) (*Supplementary information* Fig. 21). Despite our efforts,
230 no expected intermediates were observed in either mutant, likely due to their low yield.

231 Currently, there are only few enzymatic mechanisms corresponding to β-lactone ring
232 formation that have been reported,[47] including: (1) the intramolecular cyclization from seven-
233 membered ring, catalyzed by cyclase VibC in vibralactone biosynthesis;[48] (2) the tandem aldol-
234 lactonization bicyclization reaction to generate the γ-lactam-β-lactone structure, catalyzed by
235 standalone ketosynthase SalC in salinosporamide A biosynthesis;[49] (3) the β-lactone formation
236 during the intramolecular attack of the β-hydroxyl group onto the thioester carbonyl, catalyzed

237 by the C-terminal TE domain of ObiF in obafluorin biosynthesis or esterase GloD in
238 globilactone A biosynthesis;[50,51] (4) the conversion of *β*-hydroxyl to *β*-lactone, catalyzed by *β*-
239 lactone synthase OleC in olefin biosynthesis.[52,53] We proposed that the beta-lactone formation
240 in spirolactone involves a two-step oxidation to form a carboxylic acid, followed by
241 dehydration. It is likely that either the cytochrome P450 enzyme SplK or SplL is involved in
242 the process, and we also identified several genes with unknown functions, such as *splJ* and
243 *splI*. SplJ was annotated as a member of UbiD family decarboxylases, but it exhibits very
244 distinguished divergences from other proteins in this family based on sequence similarity
245 network (*Supplementary information* Fig. 22). In addition, NCBI Blastp results showed that
246 proteins homologous to SplI have not been reported to have any clear biological functions.
247 Inactivation of both genes abolished the production of spirolactone (Supplementary
248 information Fig. 21).

249 Phylogenetic analysis indicated that SplH is a separate branch and clusters with other
250 crotonyl-CoA reductase/carboxylases (CCRs) that catalyze long-chain precursors like
251 butylmalonyl-CoA and hexylmalonyl-CoA.[54,55] The previous study showed that the large
252 residue Phe380 in the CCR from *S. coelicolor* may constrain the potential pocket to accept
253 long-chain substrates, which were also found in most ethylmalonyl-CoA specific crotonyl-CoA
254 reductase/carboxylases, while its corresponding residue in SplH is smaller cysteine
255 (*Supplementary information* Fig. 23).[56] Hence, we proposed that SplH catalyzes the conversion
256 leading to the formation of 7-oxo-octylmalonyl-CoA in spirolactone, which is likely
257 synthesized from a precursor that has previously been isolated from other *Streptomyces*
258 species.[57] SplG, an O-methyltransferase homologous to AveD in avermectin biosynthesis (40%
259 identity and 55% similarity),[58] was proposed to catalyze the methylation of a hydroxyl group
260 in C-8 of spirolactone.

261 Further investigation on the key enzymes involved in the biosynthesis of spirolactone will
262 be carried out.

263 **Antifungal and cytotoxic assays of spirolactone.** Microbial *β*-lactone natural products are
264 chemically diverse and have been employed in antimicrobial, antiviral, anticancer, and
265 antiobesity therapeutics.[47] In the initial antifungal assay against *A. niger*, spirolactone
266 exhibited the strongest antifungal effect. *In vitro* antifungal susceptibility of spirolactone

267 against 34 fungal species represented by 38 clinical isolates was further tested in comparison
268 to approved antifungals using a microdilution assay according to the EUCAST protocol.
269 Spirolactone demonstrated antifungal effect against several sections of the genus *Aspergillus*
270 and the genus *Talaromyces* (Tab. 1). The lowest MICs for spirolactone were found in the
271 *Aspergillus* section *Terrei* with intrinsically high MICs for amphotericin B and in section *Usti*
272 with intrinsically high MICs for azoles. In the *Aspergillus* sections *Flavi*, *Nidulantes*, and
273 *Nigri* as well as in the genus *Talaromyces* a distinctly changed morphology of the hyphae was
274 found for all species but low MICs were observed only in some species. Only a weak effect
275 was detected for the two *Fusarium* species studied. *Aspergillus* species belonging to section
276 *Fumigati*, *Candida* spp., *Scedosporium prolificans*, *Purpureocillium lilacinum*, *Trichoderma*
277 *longibrachiatum* and Mucorales were not affected by spirolactone (*Supplementary*
278 *information* Tab. 6). Spirolactone did not exhibited cytotoxicity against the human HL-60
279 (acute promyelocytic leukemia) cell line (IC_{50} >10 µg/mL)
280 **Studies of the mechanism of action of spirolactone.** To get a clue of how spirolactone
281 functions and how it impacts *Aspergillus*, we carried out a label-free quantitative proteomics
282 analysis of model organism *A. niger* ATCC 1015. We initially cultured *A. niger* in PDB liquid
283 medium for 16 hours followed by the 1-hour and 4-hour treatment with spirolactone. The
284 proteomics analysis showed that a total of 4,447 proteins (40.4% of the total encoded proteins)
285 were detected, and 3,992 proteins (89.8% of the total detected proteins) didn't show significant
286 differences between the treatment (1-hour or 4-hour treatment with spirolactone) and the
287 control (without spirolactone treatment). Compared with the control, the abundance of 134
288 proteins significantly increased and 60 proteins significantly decreased after 1-hour
289 spirolactone treatment. In comparison, the abundance of 273 proteins significantly increased
290 and 113 proteins significantly decreased after 4-hour spirolactone treatment (Fig. 5). The
291 Cluster of Orthologous Groups (COGs) functional classification of these differential proteins
292 was performed by eggNOG-mapper v2.[59] Except for (S) function unknown, these proteins were
293 mainly clustered into a few biological processes including (Q) Secondary structure, (C) Energy
294 production and conversion, (E) Amino acid metabolism and transport, and (O) Post-
295 translational modifications, protein turnover, chaperone functions (*Supplementary information*
296 Fig. 24). The Gene Ontology (GO) annotation of these proteins was mainly involved in the

297 metabolic process, cellular process, and single-organism process during the biological process
298 (*Supplementary information* Fig. 25). Cellular component analysis showed that these proteins
299 were mainly localized intracellularly, especially in organelles. Meanwhile, most of these
300 proteins participated in catalytic activity and binding in the category of molecular function.
301 The Kyoto Encyclopedia of Genes and Genomes (KEGG) pathway enrichment analysis
302 showed that these proteins mainly participate in amino acids metabolism and purine
303 metabolism (*Supplementary information* Fig. 26).

304 Proteomic changes in fungi induced by known antifungal agents with well-described targets
305 were subsequently studied. The abundance of Erg13 (EHA22977.1, involved in ergosterol
306 biosynthesis) and manganese-superoxide dismutase (EHA27012.1, involved in oxidative stress
307 response), which was regarded as polyene antibiotic (such as amphotericin B) responsive
308 protein,[60] was not significantly altered in the presence of spirolactone. Allylamine antibiotics
309 (naftifine and terbinafine) inhibit squalene epoxidase, causing the accumulation of squalene,
310 and thereby damaging the intracellular membranes of fungi.[61] However, spirolactone is not
311 belonging to the allylamine family and didn't induce any changes in the squalene epoxidase
312 (EHA21184.1). Azoles are synthetic antifungal agents of non-natural origin that inhibit
313 cytochrome P450 sterol-14α-demethylase (CYP51) to block the ergosterol biosynthesis in the
314 fungi.[62] Similarly, spirolactone lacked the azoles substructure and had no impact on the
315 abundance of CYP51 (EHA19435.1). Natural echinocandins comprise cyclic hexapeptide and
316 lipid residues, like caspofungin, anidulafungin, and micafungin, preventing the biosynthesis of
317 glucans of the fungal cell wall through non-competitive inhibition of 1,3-β-D-glucan
318 synthase.[63] Previous proteomics analyses had proven that the level of chitinase ChiA1 in *A.*
319 *fumigatus* was significantly decreased in response to caspofungin.[64] It may represent a common
320 effect of self-resistance development due to caspofungin increased chitin content via induction
321 of chitin synthases during cell wall remodeling.[65] We did not observe the abundance of 1,3-β-
322 D-glucan synthase (EHA18547.1) and ChiA1-like chitinase (EHA28582.1) altered
323 significantly after 1-hour and 4-hour treatment of spirolactone in comparison to the control
324 group.

325 The fungal cell wall is an essential structure that maintains cell shape and protects fungi
326 against environmental stress and play roles in growth, invading ecological niches, and

327 counteracting the host immune response.[66] Fungal cell walls are composed mainly of glucans,
328 chitin, and glycoproteins, synthesized by glycosyltransferases, glycoside hydrolases, and
329 transglycosylases.[67] Congo Red Hypersensitivity (CRH) family transglycosylases are usually
330 highly expressed in multiple stages during the conidial germination of fungi and may be
331 involved in cell wall synthesis and stability. The volcano plot of differential proteins indicated
332 that a CRH family transglycosylase (EHA23738.1) was significantly inhibited, suggesting
333 spirolactone might interfere with the formation of the fungal cell wall. Trehalose-6-phosphate
334 synthase/phosphatase is another important enzyme for cell wall integrity and fungal virulence
335 in various *Aspergillus* species.[68] The relative abundance of trehalose 6-phosphate synthase
336 (EHA27700.1) was also significantly decreased after spirolactone treatment. The above data
337 indicated that the mode of action of spirolactone could be through disruption of fungal cell wall
338 biosynthesis and stability (Fig. 4). Besides, we found that the two enzymes Erg24
339 (EHA26587.1) and Erg27 (EHA20711.1), which catalyze the biosynthesis of 4,4-
340 dimethylcholesta-8,14,24-trienol to fecosterol,[69] were remarkably upregulated after
341 spirolactone treatment (Fig. 4). Drug efflux and resistance in fungi could be mediated by ATP-
342 binding cassette (ABC) transporters, such as CDR1 was induced to high expression in *A.*
343 *fumigatus* AF293 in the presence of azole antibiotics.[70] The expression of an ABC transporter
344 (EHA25684.1) was activated after spirolactone treatment. We observed the abundance of
345 several putative spirolactone-responsive proteins were significantly altered. For example, the
346 relative abundance of several proteins including inositol hexaphosphate kinase KCS1
347 (EHA27881.1), ubiquitin-protein ligase ASI3 (EHA19328.1), mitochondrial phosphate carrier
348 protein PIC2 (EHA22842.1), pyridoxamine 5'-phosphate oxidase (EHA19800.1) and
349 glucohydrolase (EHA21384.1) was significantly increased, but oxygen-dependent FAD-linked
350 oxidoreductase (EHA22577.1) and dienelactone hydrolase (EHA27638.1) was significantly
351 decreased in spirolactone-treated samples. Interestingly, an amount of unknown function
352 proteins was found to increase or decrease in abundance affected by spirolactone and their
353 functions still need to be further explored.
354
355 **Conclusion**

356 Herein, we report the discovery of a novel class of antifungal agent spirolactone, featuring an
357 unprecedented carbon skeleton. Spirolactone exhibits selective antifungal activities against
358 several pathogenic *Aspergillus* species, some of which are intrinsically resistant to
359 amphotericin B or azoles, as well as against *Talaromyces* species. We confirmed the BGC of
360 spirolactone through a variety of in silico and *in vivo* analyses. Proteomics data revealed that
361 treatment with spirolactone leads to the inhibition of transglycosylase and trehalose-6-
362 phosphate synthase/phosphatase, suggesting that it may target fungal cell wall biosynthesis.
363

364 **Methods and Materials**

365 **Strains, plasmids, and culture conditions.** All strains and plasmids used in this study were
366 summarized in *Supplementary information* Tab. 5. All primers used in this study were
367 summarized in *Supplementary information* Tab. 6. All constructed *E. coli* strains were growing
368 on lysogeny broth (LB) liquid or agar medium at 37 °C. Wild-type *Streptomyces* strains and its
369 mutants were cultivated on Mannitol Soya Flour (MS) agar medium (20.0 g mannitol, 20.0 g
370 soya flour, 20.0 g agar, 1.0 L tap water, pH=7.0-7.5) at 30 °C. The small-scale fermentation of
371 *Streptomyces* strains was using 50 mL MS liquid medium in 250 mL flask, shaking at 200 rpm,
372 30 °C for 7 days. The large-scale fermentation of *Streptomyces* strains were carried out in
373 medium 2 ($CaCl_2 \cdot 2H_2O$, 3.0 g; citric acid/Fe III, 1.0 g; $MnSO_4 \cdot H_2O$, 0.2 g; $ZnCl_2$, 0.1 g;
374 $CuSO_4 \cdot 5H_2O$, 0.025 g; $Na_2B_4O_7 \cdot 10H_2O$, 0.02 g; $Na_2MoO_4 \cdot 2H_2O$, 0.01 g; and oatmeal, 20.0 g,
375 in 1.0 L distilled water), at 200 L scale in a 300 L fermentation vessel, for 6 days with aeration
376 of 25-50 L min^{-1}, stirring at 200 rpm, 28 °C, with a pH range of 5.4-6.4. Antibiotics such as
377 apramycin (50 mg mL^{-1}), kanamycin (50 mg mL^{-1}) or chloramphenicol (25 mg mL^{-1}) were
378 appropriately used for resistance selection.
379

380 **Genomic DNA extraction, sequencing, and assembly.** The *S. iranensis* culture was growing
381 in 50 mL sterilized liquid ISP2 medium (yeast extract 4.0 g; malt extract 10.0 g; and dextrose
382 4.0 g in 1.0 L distilled water, pH = 7.2) in 250 mL flask at 30 °C and 160 rpm for 5 days to
383 generate sufficient biomass. The genomic DNA of *S. iranensis* was isolated using the QIAGEN
384 Genomic-tip 20/G kit using a modified protocol and grinding with a mortar and pestle
385 submerged in liquid nitrogen.[71] The procedure of genomic DNA sequencing was combining

386 Oxford Nanopore Technologies MinION and Illumina MiSeq systems. To generate the
387 nanopore data, both the SQK-RBK004 and the SKQ-RBK110-96 rapid barcoding kits were
388 used for construction of three libraries, which were sequenced on two separate 9.4.1 flowcells.
389 The *de novo* assembly was performed using Flye (v2.9-b1768) with the parameters --nano-hq
390 --t 12. Since the genome could not be fully resolved using existing assemblers, the Terminal
391 inverted repeat edge from the unambiguous assembly repeat graph were manually attached to
392 both ends of the chromosome edge and the orientations were verified by mapping of the reads
393 on the new assembly and manual inspection. This approach was later suggested by the Flye
394 assembler Misha. The Unicycler (v0.4.8) polishing module was used to polish the nanopore
395 assembly with illumina data.
396
397 **Genetic manipulation.** To verify the BGC of spirolactone and its individual biosynthetic
398 genes, the classical CRISPR-Cas9 method, and advanced CRISPR-cBEST base editing toolkit
399 were used to construct gene-inactive mutants.[36] The function-specific plasmids
400 (Supplementary information Tab. 7) were constructed according to the respective protocol
401 followed by introducing into wild-type *S. iranensis* HM 35 by conjugation with donor strain
402 ET12567/pUZ8002 on SFM solid medium (soya flour 20.0 g; mannitol 20.0 g; and bacteria
403 agar 20.0 g, in 1.0 L distilled water, pH = 7.2) according to modified protocol. The
404 exconjugants after resistance screening (50 μg mL^{-1} apramycin and 25 μg mL^{-1} nalidixic acid)
405 were further verified by DNA extraction, PCR reaction, and Sanger sequencing.
406 DNA polymerases (Q5® High-Fidelity 2X Master Mix with Standard Buffer and OneTaq®
407 2X Master Mix with Standard Buffer) and restriction enzymes (NcoI, EcoRI) were purchased
408 from New England Biolabs. PCR amplifications and restriction enzyme digestions were carried
409 out on Bio-Rad's thermal cyclers according to the manufacturer's instructions. Plasmid DNA
410 extraction was performed using NucleoSpin Plasmid EasyPure Kit (Macherey-Nagel,
411 Germany). DNA purification was conducted on 1% Tris-acetate-EDTA (TAE) agarose gel
412 followed by using NucleoSpin Gel and PCR Clean-up Kits (Macherey-Nagel, Germany). One
413 Shot™ Mach1™ T1 Phage-Resistant Chemically Competent *E. coli* from Invitrogen™ was
414 used for transformation. All oligonucleotides were ordered from Integrated DNA Technologies
415 (Supplementary information Tab. 8) and Sanger sequencing was offered by Eurofins

416 Genomics (Luxembourg). All solvents used for chromatography and HR-MS were purchased
417 from VWR Chemicals with LC-MS grade, while for metabolites extraction, the solvents were
418 of HPLC grade.
419
420 **HR-ESI-MS analysis.** HR-ESI-MS analysis was carried out via ultra-high-performance liquid
421 chromatography-diode array detection–quadrupole time-of-flight mass spectrometry (UHPLC-
422 DAD-QTOFMS) depending on an Agilent Infinity 1290 UHPLC system equipped with a diode
423 array detector. Separation was achieved on a 250 × 2.1 mm i.d., 2.7 µm, Poroshell 120 Phenyl
424 Hexyl column (Agilent Technologies) held at 60 °C. The sample, 1 µL, was eluted at a flow
425 rate of 0.35 mL min^{-1} using a linear gradient from 10% acetonitrile in Milli-Q water buffered
426 with 20 mM formic acid increasing to 100% in 15 min, staying there for 2 min before returning
427 to 10% in 0.1 min. Starting conditions were held for 3 min before the following run. MS
428 detection was performed on an Agilent 6545 QTOF MS equipped with Agilent Dual Jet Stream
429 ESI with a drying gas temperature of 160 °C, a gas flow of 13 L min^{-1}, sheath gas temperature
430 of 300 °C and flow of 16 L min^{-1}. Capillary voltage was set to 4000 V and nozzle voltage to
431 500 V in positive mode. All data were processed using Agilent MassHunter Qualitative
432 Analysis software (Agilent Technologies, USA).
433
434 **Large-scale fermentation and isolation.** The culture broth from large-scale fermentation
435 (described above) was filtered and loaded onto an Amberchrom 161c resin LC column (200 ×
436 20 cm, 6 L). Elution with a linear gradient of H_2O-MeOH (from 30% to 100% v/v, flow rate
437 0.5 L min^{-1}, in 58 min) afforded seven fractions (Fr.A-Fr.G). Fr.G was first fractionated by
438 silica gel chromatography with a CH_2Cl_2-CH_3OH gradient to yield 16 fractions, Fr.1-Fr.16.
439 Fr.7 was further separated by a Sephadex LH-20 (MeOH) column, and twelve sub-fractions
440 were obtained. The sub-fractions were separated by semipreparative HPLC RP-C18 (MeCN-
441 H_2O as gradient) to afford compound **1.**
442 Spirolactone (**1**): white solid; $[\alpha]_D^{25}$ 15 (0.1 mg/mL, CH_3OH), UV/vis (CH_3CN/H_2O) λ_{max}
443 230, 270 nm; ECD λ_{ext} (Δε) (CH_3OH) 235 (–9.78), 267 (7.02), 301 (–3.31) nm; IR (ATR) ν_{max}
444 2932, 2748, 2704, 1810, 1713, 1686, 1619, 1457, 1382, 1173, 1134, 1085, 1057, 1013, 991,
445 947 cm^{-1}; (-)-HR-ESI-MS *m/z* 881.4659 $[M + Na]^+$ (calcd for $C_{47}H_{70}O_{14}$, 881.4658).

446

447 **NMR spectroscopy.** NMR spectra were recorded on 800 MHz Bruker Avance III spectrometer
448 equipped with a TCI CryoProbe using standard pulse sequences. Measurements were carried
449 out using ^{1}H and ^{13}C NMR, ^{1}H-^{13}C heteronuclear single quantum coherence (HSQC), ^{1}H-^{13}C
450 heteronuclear multiple bond correlation (HMBC), ^{1}H-^{1}H correlation spectroscopy (COSY),
451 ^{1}H-^{1}H nuclear overhauser effect spectroscopy (NOESY). Chemical shifts (δ) were reported in
452 parts per million (ppm) and referenced to the solvent signals. Data are described as follows:
453 chemical shift, multiplicity (*br* = broad, *s* = singlet, *d* = doublet, *t* = triplet, *dd* = doublet of
454 doublet, *m* = multiplet and *ov* = overlapped) and coupling constants (in hertz). All NMR data
455 were processed using MestReNova 14.0.

456

457 **Crystal Data for spirolactone.** The suitable crystal was selected and mounted in a nylon loop
458 directly from the ethanol suspension and frozen in liquid nitrogen on a Synchrotron
459 diffractometer. X-ray data collection of **1** was performed on an Agilent Supernova
460 Diffractometer using CuKα radiation, and the crystal was kept at 100 K during data collection.
461 Using Olex2,[72] the structure was solved with the XT[73] structure solution program using
462 Intrinsic Phasing and refined with the SHELXL[74] refinement package using Least Squares
463 minimization. Crystal data for $C_{47}H_{70}O_{14}$ (M =859.03 g/mol): monoclinic, space group $P2_1$ (no.
464 4), a = 10.118(7) Å, b = 16.799(7) Å, c = 14.081(5) Å, β = 103.385(12)°, V = 2328(2) Å^3, Z =
465 2, T = 100 K, μ (synchrotron) = 0.089 mm^{-1}, $Dcalc$ = 1.225 g/cm^3, 17409 reflections measured
466 (3.836° ≤ 2θ ≤ 45.2°), 5762 unique (R_{int} = 0.0646, R_{sigma} = 0.0641) which were used in all
467 calculations. The final R_1 was 0.0646 (I > 2σ(I)) and wR_2 was 0.1523 (all data).

468

469 **Sample preparation for proteomics analysis.** Approximately 1.0 x 10^7 conidia mL^{-1} of *A.*
470 *niger* ATCC 1015 strain were used to inoculate 100 mL (three biological replicates) of liquid
471 cultures (PDB) in 1 L flask that were incubated in a reciprocal shaker at 28 °C in 180 rpm for
472 16 hours. Afterwards, samples in the treatment group were treated with 0.2 µg (concentration
473 of 2 ng/mL) of spirolactone for 1-hour and 4-hour. Mycelia were then harvested by filtering,
474 washed thoroughly with sterile water and quickly frozen in liquid nitrogen. Pellets were lysed
475 in 100 µL lysis buffer (6 M Guanidium Hydrochloride, 10 mM TCEP, 40 mM CAA, 50 mM

476 HEPES, pH 8.5) by boiling the samples at 95 °C for 5 mins, sonicating on high for 5 x 60 sec
477 on/30sec off using the bioruptor pico sonication water bath (Diagenode) and finally disrupting
478 twice with the tissuelyser (QIAGEN) going from 3 to 30 Hz in 1 min. Lysed samples were
479 centrifuged at 18,000 g for 10 mins, and supernatants were transferred to clean LoBind
480 Eppendorf tubes. Protein concentration was determined by BCA rapid gold (Thermo) and 10
481 µg of protein was taken forward for digestion. Samples were diluted 1:3 with digestion buffer
482 (10% acetonitrile in 50mM HEPES pH 8.5) and incubated with 1:100 enzyme to protein ratio
483 of LysC (MS Grade, Wako) at 37 °C for 4 hours. Samples were further diluted to a final 1:10
484 with more digestion buffer and digested with 1:100 trypsin for 18 hours at 37 °C. After
485 digestion, samples were acidified with TFA and desalted using the SOLAµ™ SPE plate (HRP,
486 Thermo).[75] Between each application, the solvents were spun through by centrifugation at
487 1,500 rpm. For each sample, the filters were activated with 200 µL of 100% Methanol, then
488 200 µL of 80% Acetonitrile, 0.1% formic acid. The filters were subsequently equilibrated 2x
489 with 200 µL of 1% TFA, 3% acetonitrile, after which the sample was loaded. After washing
490 the tips twice with 200 µL of 0.1% formic acid, the peptides were eluted into clean 0.5 mL
491 Eppendorf tubes using 40% acetonitrile, 0.1% formic acid. The eluted peptides were
492 concentrated in an Eppendorf Speedvac. Samples were reconstituted in 12 µL A* buffer with
493 iRT peptides (Biognosys).
494
495 **MS analysis for proteomics analysis.** Peptides were loaded onto a 2cm C18 trap column
496 (ThermoFisher 164946), connected in-line to a 15cm C18 reverse-phase analytical column
497 (Thermo EasySpray ES904) using 100% Buffer A (0.1% Formic acid in water) at 750 bar,
498 using the Thermo EasyLC 1200 HPLC system, and the column oven operating at 30°C.
499 Peptides were eluted over a 70 minutes gradient ranging from 10% to 60% of Buffer B (80%
500 acetonitrile, 0.1% formic acid) at 250 µL/min, and the Orbitrap Exploris instrument (Thermo
501 Fisher Scientific) was run in DIA mode with FAIMS ProTM Interface (ThermoFisher
502 Scientific) with CV of -45 V. Full MS spectra were collected at a resolution of 120,000, with
503 an AGC target of 300% or maximum injection time set to 'auto' and a scan range of 400–1000
504 m/z. The MS2 spectra were obtained in DIA mode in the orbitrap operating at a resolution of
505 60.000, with an AGC target 1000% or maximum injection time set to 'auto', a normalised HCD

506 collision energy of 32. The isolation window was set to 6 m/z with a 1 m/z overlap and window
507 placement on. Each DIA experiment covered a range of 200 m/z resulting in three DIA
508 experiments (400-600 m/z, 600-800 m/z and 800-1000 *m/z*). Between the DIA experiments a
509 full MS scan is performed. MS performance was verified for consistency by running complex
510 cell lysate quality control standards, and chromatography was monitored to check for
511 reproducibility.
512
513 **Data process for proteomics analysis.** The raw files were analyzed using Spectronaut™
514 (version 17.4) spectra were matched against the reviewed *A. niger* ATCC 1015 NCBI database.
515 Dynamic modifications were set as Oxidation (M) and Acetyl on protein N-termini. Cysteine
516 carbamidomethyl was set as a static modification. All results were filtered to a 1% FDR, and
517 protein quantitation done on the MS1 level. Only proteotypic peptides were used for
518 quantification and protein groups were inferred by IDPicker.
519
520 **Antifungal susceptibility testing.** In vitro antifungal susceptibility of spirolactone against 34
521 fungal species represented by 38 clinical isolates was tested in comparison to approved
522 antifungals amphotericin B (AMB; European Pharmacopoeia, Strasbourg, France);
523 itraconazole (ITZ), and voriconazole (VCZ; Pfizer Inc., Peapack, NJ, USA) by using the broth
524 microdilution technique following the European Committee on Antimicrobial Susceptibility
525 Testing (EUCAST) standard methodology for yeasts or filamentous fungi respectively, in the
526 main parts. In contrast to the EUCAST protocol, microdilution plates were prepared by 2-fold
527 serial dilutions of the antifungal agents. Filamentous fungi were grown on malt extract agar
528 (MEA) for 2 to 7 days at 35 °C and yeasts were cultivated on yeast extract peptone dextrose
529 agar (YPD) for 24 hours. Spore or yeast cell suspensions were counted with a hemocytometer.
530 Minimum inhibitory concentrations (MIC) endpoints of filamentous fungi were defined as
531 100% reduction in growth and were determined visually using a mirror after 48 h of incubation
532 at 35 °C. Microdilution plates of yeasts were read with a microdilution plate reader (Infinite®
533 M Nano plus, Tecan) and MIC endpoints were defined as the lowest drug concentration giving
534 inhibition of growth of ≥ 50% of that of the drug-free control. Since the mode of action of
535 spirolactone is unknown, the minimum effective concentration (MEC) was determined as well

536 by reading the microplates with the aid of an inverted microscope (Eclipse Ts2, Nikon). *A.*
537 *fumigatus* ATCC 204305 and *Candida parapsilosis* ATCC 22019 were used as reference
538 strains.[76,77]
539
540 **Cytotoxic activities of spirolactone.** Cytotoxicity against the human cell line HL-60 was
541 evaluated using Alamar Blue (Thermos Scientific, Kansas, USA). The assay (Hamid et al.
542 2004) was performed in 96 well plates (Costar 3595, Corning, New York, USA), with an assay
543 volume of 200 μL. The software Prism 5.03 was used for data analysis (GraphPad Software,
544 USA).[78]
545
546 **Data availability.** The genome sequence of *S. iranensis* HM35 has been deposited in the NCBI
547 under BioProject accession number PRJNA1026072 and BioSample accession number
548 SAMN37733152. The genome sequence can be found under Genbank accession number
549 CP136563. The crystal data of spirolactone was deposited in CCDC database
550 (https://www.ccdc.cam.ac.uk/) with accession number 2178562. The metabolomics data of
551 wild-type and mutant strains has been deposited in the MassIVE repository
552 (https://massive.ucsd.edu/) under identifier MSV 000094394. The mass spectrometry for
553 proteomics analysis have been deposited in the ProteomeXchange Consortium
554 (https://www.proteomexchange.org/) with data set identifier MassIVE MSV 000094235. The
555 NMR data were deposited at NP-MRD, NP0332733.
556
557 **Acknowledgements**
558 L.D. acknowledges funding from DTU Skylab, Novo Nordisk Foundation (Grant
559 NNF23OC0082881) and Innovation Fund Denmark (Grant 3141-00013A). M.H.C.
560 acknowledges funding for the DTU Screening Core from the Novo Nordisk Foundation (Grant
561 NNF19OC0055818) and the Carlsberg Foundation (Grant CF19-0072). Y.Q. acknowledges
562 funding from Novo Nordisk Foundation (NNF22OC0079928). The NMR Center DTU and the
563 Villum Foundation are acknowledged for access to the 800 MHz spectrometer. The
564 metabolomic data was generated at DTU Metabolomics Core facilities with help of Dr. A.
565 Andersen. Thanks to Prof. Mohamed Shaaban for repurification of spirolactone and recording
566 the ECD spectrum. Thanks to Prof. Jacob Blæsbjerg Hoof for the *A. niger* strain and advice.
567

568 **Competing interests**

569 The authors declare that there are no competing interests. Two patent applications were filed
570 with the numbers of PCT/EP2023/067953 and EP24150176.6.

571

572 **Additional Information**

573 **Supplementary information:** The online version contains supplementary material available
574 at xxx.

575 **Correspondence and requests** for materials should be addressed to Ling Ding.

576

577 **References**

578 1. Brown, G. D., et al. Hidden killers: human fungal infections. *Sci. Transl. Med.* **4**, 165rv13
579 (2012).
580 2. Bongomin, F., Gago, S., Oladele, R. O. & Denning, D. W. Global and multi-national
581 prevalence of fungal diseases-estimate precision. *J. Fungi.* **3**, 57 (2017).
582 3. Denning, D. W. Global incidence and mortality of severe fungal disease. *Lancet Infect.*
583 *Dis.* **S1473-3099**, 00692-8 (2024).
584 4. Sarden, N., et al. A B1a-natural IgG-neutrophil axis is impaired in viral- and steroid-
585 associated aspergillosis. *Sci. Transl. Med.* **14**, eabq6682 (2022).
586 5. Osherov, N. & Kontoyiannis, D. P. The anti-*Aspergillus* drug pipeline: Is the glass half
587 full or empty? *Med. Mycol.* **55**, 118-124 (2017).
588 6. Hoenigl, M., et al. The antifungal pipeline: fosmanogepix, ibrexafungerp, olorofim,
589 opelconazole, and rezafungin. *Drugs* **81**, 1703-1729 (2021).
590 7. Perfect, J. R. The antifungal pipeline: a reality check. *Nat. Rev. Drug Discovery* **16**, 603-
591 616 (2017).
592 8. Denning, D. W. & Bromley, M. J. Infectious Disease. How to bolster the antifungal
593 pipeline. *Science* **347**, 1414-1416 (2015).
594 9. Gubbins, P. O. & Amsden, J. R. Drug-drug interactions of antifungal agents and
595 implications for patient care. *Expert Opin. Pharmacother.* **6**, 2231-2243 (2005).
596 10. Rhodes, J., et al. Population genomics confirms acquisition of drug-resistant *Aspergillus*
597 *fumigatus* infection by humans from the environment. *Nat. Microbiol*. **7**, 663-674 (2022).

598 11. Vermeulen, E., Lagrou, K. & Verweij, P. E. Azole resistance in *Aspergillus fumigatus*: a
599 growing public health concern. *Curr. Opin. Infect. Dis.* **26**, 493-500 (2013).
600 12. Zhou, D., et al. Extensive genetic diversity and widespread azole resistance in greenhouse
601 populations of *Aspergillus fumigatus* in Yunnan, China. *mSphere* **6**, e00066-21 (2021).
602 13. Newman, D. J. & Cragg, G. M. Natural products as sources of new drugs over the nearly
603 four decades from 01/1981 to 09/2019. *J. Nat. Prod.* **83**, 770-803 (2020).
604 14. Jiang, T., Pu, H., Duan, Y., Yan, X. & Huang, Y. New natural products of *Streptomyces*
605 sourced from deep-sea, desert, volcanic, and polar regions from 2009 to 2020. *Chin. J.*
606 *Org. Chem.* **41**, 1804-1820 (2021).
607 15. Alam, K., et al. *Streptomyces*: The biofactory of secondary metabolites. *Front. Microbiol.*
608 **13**, 968053 (2022).
609 16. Hazen, E. L. & Brown, R. Fungicidin, an antibiotic produced by a soil Actinomycete. *Proc.*
610 *Soc. Exp. Biol. Med.* **76**, 93-97 (1951).
611 17. Oura, M., Sternberg, T. H. & Wright, E. T. A new antifungal antibiotic, amphotericin B.
612 *Antibiot. Annu.* **3**, 566-573 (1955).
613 18. Anderson, T. M., et al. Amphotericin forms an extramembranous and fungicidal sterol
614 sponge. *Nat. Chem. Biol.* **10**, 400-406 (2014).
615 19. Lewandowska, A., et al. Fungicidal amphotericin B sponges are assemblies of staggered
616 asymmetric homodimers encasing large void volumes. *Nat. Struct. Mol. Biol.* **28**, 972-981
617 (2021).
618 20. Gray, K. C., et al. Amphotericin primarily kills yeast by simply binding ergosterol. *Proc.*
619 *Natl. Acad. Sci. USA* **109**, 2234-2239 (2012).
620 21. Hamill, R. J. Amphotericin B formulations: a comparative review of efficacy and toxicity.
621 *Drugs* **73**, 919-934 (2013).
622 22. Fanos, V. & Cataldi, L. Amphotericin B-induced nephrotoxicity: A review. *J. Chemother.*
623 **12**, 463-470 (2000).
624 23. Chen, R., et al. Turonicin A, an antifungal linear polyene polyketide from an Australian
625 *Streptomyces* sp. *J. Nat. Prod.* **86**, 2054-2058 (2023).

626 24. Tchize Ndejouong, B., et al. Hygrobafilomycin, a cytotoxic and antifungal macrolide
627 bearing a unique monoalkylmaleic anhydride moiety, from *Streptomyces varsoviensis*. *J.*
628 *Antibiot.* **63**, 359-363 (2010).
629 25. Zhang, Z. W., Zhou, T., Harunari, E., Oku, N. & Igarashi, Y. Iseolides A-C, antifungal
630 macrolides from a coral-derived actinomycete of the genus *Streptomyces*. *J. Antibiot.* **73**,
631 534-541 (2020).
632 26. Chevrette, M. G., et al. The antimicrobial potential of *Streptomyces* from insect
633 microbiomes. *Nat. Commun.* **10**, 516 (2019).
634 27. Arai, M. Isolation of three main components. F3, F4 and F5, from azalomycin F-complex.
635 *J. Antibiot.* **23**, 107-112 (1970).
636 28. Chen, Y., et al. Discovery of niphimycin C from *Streptomyces yongxingensis* sp. nov. as a
637 promising agrochemical fungicide for controlling banana *Fusarium* Wilt by destroying the
638 mitochondrial structure and function. *J. Agric. Food Chem.* **70**, 12874-12795 (2022).
639 29. Zhang, Y., et al. Antifungal activities of metabolites produced by a termite-associated
640 *Streptomyces canus* BYB02. *J. Agric. Food Chem.* **61**, 1521-1524 (2013).
641 30. Nguyen, C. T., Dhakal, D., Pham, V. T. T., Nguyen, H. T. & Sohng, J. K. Recent advances
642 in strategies for activation and discovery/characterization of cryptic biosynthetic gene
643 clusters in *Streptomyces*. *Microorganisms* **8**, 616 (2020).
644 31. Ziemert, N., Alanjary, M. & Weber, T. The evolution of genome mining in microbes - a
645 review. *Nat. Prod. Rep.* **33**, 988-1005 (2016).
646 32. Hamedi, J., et al. *Streptomyces iranensis* sp nov., isolated from soil. *Int. J. Syst. Evol.*
647 *Microbiol.* **60**, 1504-1509 (2010).
648 33. Yang, Z., et al. *Streptomyces* alleviate abiotic stress in plant by producing pteridic acids.
649 *Nat. Commun.* **14**, 7398 (2023).
650 34. Blin, K., et al. antiSMASH 7.0: new and improved predictions for detection, regulation,
651 chemical structures and visualisation. *Nucleic Acids Res.* **51**, W46-W50 (2023).
652 35. Kautsar, S. A., et al. BiG-FAM: the biosynthetic gene cluster families database. *Nucleic*
653 *Acids Res.* **49**, D490-D497 (2021).
654 36. Tong, Y., et al. CRISPR-Cas9, CRISPRi and CRISPR-BEST-mediated genetic
655 manipulation in streptomycetes. *Nat. Protoc.* **15**, 2470-2502 (2020).

656 37. Keatinge-Clay, A. T. The structures of type I polyketide synthases. *Nat. Prod. Rep.* **29**,
657 1050-1073 (2012).
658 38. Wang, J., et al. Platensimycin is a selective FabF inhibitor with potent antibiotic properties.
659 *Nature* **441**, 358-361 (2006).
660 39. Keatinge-Clay, A. T. A tylosin ketoreductase reveals how chirality is determined in
661 polyketides. *Chem. Biol.* **14**, 898-908 (2007).
662 40. Gehret, J. J., et al. Terminal alkene formation by the thioesterase of curacin a biosynthesis
663 structure of a decarboxylating thioesterase. *J. Biol. Chem.* **286**, 14445-14454 (2011).
664 41. Rudolf, J. D., Chang, C. Y., Ma, M. & Shen, B. Cytochromes P450 for natural product
665 biosynthesis in *Streptomyces*: sequence, structure, and function. *Nat. Prod. Rep.* **34**, 1141-
666 1172 (2017).
667 42. Moebius, N., et al. Biosynthesis of the respiratory toxin bongkrekic acid in the pathogenic
668 bacterium *Burkholderia gladioli*. *Chem. Biol.* **19**, 1164-1174 (2012).
669 43. Zhang, Q., et al. Carboxyl formation from methyl via triple hydroxylations by XiaM in
670 xiamycin A biosynthesis. *Org. Lett.* **14**, 6142-6145 (2012).
671 44. Aparicio, J. F., Caffrey, P., Gil, J. A. & Zotchev, S. B. Polyene antibiotic biosynthesis gene
672 clusters. *Appl. Microbiol. Biotechnol.* **61**, 179-188 (2003).
673 45. Chen, S., et al. Tailoring the P450 monooxygenase gene for FR-008/Candicidin
674 biosynthesis. *Appl. Environ. Microbiol.* **75**, 1778-1781 (2009).
675 46. Yang, J., Qi, Y., Blodgett, J. & Wencewicz, T. Multifunctional P450 monooxygenase CftA
676 diversifies the clifednamide pool through tandem C-H bond activations. *J. Nat. Prod.* **85**,
677 47-55 (2022).
678 47. Robinson, S. L., Christenson, J. K. & Wackett, L. P. Biosynthesis and chemical diversity
679 of β-lactone natural products. *Nat. Prod. Rep.* **36**, 458-475 (2019).
680 48. Feng, K. N., et al. A hydrolase-catalyzed cyclization forms the fused bicyclic β-Lactone in
681 vibralactone. *Angew. Chem. Int. Ed.* **59**, 7209-7213 (2020).
682 49. Bauman, K. D., et al. Enzymatic assembly of the salinosporamide γ-lactam-β-lactone
683 anticancer warhead. *Nat. Chem. Biol.* **18**, 538-546 (2022).

684 50. Schaffer, J. E., Reck, M. R., Prasad, N. K. & Wencewicz, T. A. β-Lactone formation during
685 product release from a nonribosomal peptide synthetase. *Nat. Chem. Biol.* **13**, 737-744
686 (2017).
687 51. Xu, Z. F., et al. Discovery and biosynthetic pathway analysis of cyclopentane-β-lactone
688 globilactone A. *Nat. Synth.* **3**, 99-110 (2024).
689 52. Christenson, J. K., et al. β-Lactone synthetase found in the olefin biosynthesis pathway.
690 *Biochemistry* **56**, 348-351 (2017).
691 53. Robinson, S. L., et al. Mechanism of a standalone β-lactone synthetase: new continuous
692 assay for a widespread ANL superfamily enzyme. *ChemBioChem* **20**, 1701-1711 (2019).
693 54. Chan, Y. A., Podevels, A. M., Kevany, B. M. & Thomas, M. G. Biosynthesis of polyketide
694 synthase extender units. *Nat. Prod. Rep.* **26**, 90-114 (2009).
695 55. Wilson, M. C. & Moore, B. S. Beyond ethylmalonyl-CoA: The functional role of crotonyl-
696 CoA carboxylase/reductase homologs in expanding polyketide diversity. *Nat. Prod. Rep.*
697 **29**, 72-86 (2012).
698 56. Quade, N., Huo, L. J., Rachid, S., Heinz, D. W. & Muller, R. Unusual carbon fixation gives
699 rise to diverse polyketide extender units. *Nat. Chem. Biol.* **8**, 117-124 (2012).
700 57. Omura, S., Imai, H., Takeshima, H., & Nakagawa, A. Structure of a new antimicrobial
701 unsaturated fatty acid from *Sm. kitasatoenis* NU-23-1. *Chem. Pharm. Bull.* 24(12), 3139-
702 3143 (1976).
703 58. Ikeda, H. & Omura, S. Avermectin biosynthesis. *Chem. Rev.* **97**, 2591-2610 (1997).
704 59. Cantalapiedra, C. P., Hernández-Plaza, A., Letunic, I., Bork, P. & Huerta-Cepas, J.
705 eggNOG-mapper v2: Functional annotation, orthology assignments, and domain prediction
706 at the metagenomic scale. *Mol. Biol. Evol.* **38**, 5825-5829 (2021).
707 60. Gautam, P., et al. Proteomic and transcriptomic analysis of *Aspergillus fumigatus* on
708 exposure to amphotericin B. *Antimicrob. Agents Chemother.* **52**, 4220-4227 (2008).
709 61. Ghannoum, M., et al. *In vitro* antifungal activity of naftifine hydrochloride against
710 dermatophytes. *Antimicrob. Agents Chemother.* **57**, 4369-4372 (2013).
711 62. Hitchcock, C. A. Cytochrome-P-450-dependent 14α-sterol demethylase of *Candida*
712 *albicans* and its interaction with azole antifungals. *Biochem. Soc. Trans.* **19**, 782-787
713 (1991).

714 63. Sawistowska-Schröder, E. T., Kerridge, D. & Perry, H. Echinocandin inhibition of 1,3-*β*-
715 D-glucan synthase from *Candida albicans*. *FEBS Lett.* **173**, 134-138 (1984).
716 64. Cagas, S. E., Jain, M. R., Li, H. & Perlin, D. S. Profiling the *Aspergillus fumigatus* proteome
717 in response to caspofungin. *Antimicrob. Agents Chemother.* **55**, 146-154 (2011).
718 65. Walker, L. A., Gow, N. A. R. & Munro, C. A. Elevated chitin content reduces the
719 susceptibility of *Candida* species to caspofungin. *Antimicrob. Agents Chemother.* **57**, 146-
720 154 (2013).
721 66. Garcia-Rubio, R., de Oliveira, H. C., Rivera, J. & Trevijano-Contador, N. The fungal cell
722 wall: *Candida*, *Cryptococcus*, and *Aspergillus* species. *Front. Microbiol.* **10**, 2993 (2020).
723 67. Fang, W., et al. Mechanisms of redundancy and specificity of the *Aspergillus fumigatus*
724 Crh transglycosylases. *Nat. Commun.* **10**, 1669 (2019).
725 68. Puttikamonkul, S., et al. Trehalose 6-phosphate phosphatase is required for cell wall
726 integrity and fungal virulence but not trehalose biosynthesis in the human fungal pathogen
727 *Aspergillus fumigatus*. *Mol. Microbiol.* **77**, 891-911 (2010).
728 69. Dhingra, S. & Cramer, R. A. Regulation of sterol biosynthesis in the human fungal
729 pathogen *Aspergillus fumigatus*: opportunities for therapeutic development. *Front.*
730 *Microbiol.* **8**, 92 (2017).
731 70. Fraczek, M. G., et al. The *cdr1B* efflux transporter is associated with non-*cyp51a*-mediated
732 itraconazole resistance in *Aspergillus fumigatus*. *J. Antimicrob. Chemother.* **68**, 1486-1496
733 (2013).
734 71. Alvarez-Arevalo, M., et al. Extraction and Oxford Nanopore sequencing of genomic DNA
735 from filamentous Actinobacteria. *STAR protoc.* **4**, 101955 (2023).
736 72. Dolomanov, O. V., et al. *OLEX2*: a complete structure solution, refinement and analysis
737 program. *J. Appl. Crystallogr.* **42**, 339-341 (2009).
738 73. Sheldrick, G. M. Crystal structure refinement with SHELXL. *Acta Crystallogr C Struct.*
739 *Chem.* **71**, 3-8 (2015).
740 74. Sheldrick, G. M. SHELXT - integrated space-group and crystal-structure determination.
741 *Acta Crystallogr. A Found. Adv.* **71**, 3-8 (2015).

742 75. Rappsilber, J., Mann, M. & Ishihama, Y. Protocol for micro-purification, enrichment, pre-
743 fractionation and storage of peptides for proteomics using StageTips. *Nat. Protoc*. **2**, 1896-
744 1906 (2007).
745 76. Arendrup, M. C., Cuenca-Estrella, M., Lass-Flörl, C., Hope, W. & EUCAST-AFST.
746 EUCAST technical note on the EUCAST definitive document EDef 7.2: Method for the
747 determination of broth dilution minimum inhibitory concentrations of antifungal agents for
748 yeasts EDef 7.2 (EUCAST-AFST). *Clin. Microbiol. Infect.* **18**, E246-247 (2012).
749 77. Subcommittee on Antifungal Susceptibility Testing of the ESCMID European Committee
750 for Antimicrobial Susceptibility Testing. EUCAST Technical Note on the method for the
751 determination of broth dilution minimum inhibitory concentrations of antifungal agents for
752 conidia forming moulds. *Clin. Microbiol. Infect.* **14**, 982-984 (2008).
753 78. Lima, T. S., et al. Molecular profiling of docetaxel-resistant prostate cancer cells identifies
754 multiple mechanisms of therapeutic resistance. *Cancers* **13**, 1290 (2021).
755
756

757 **Tab. 1** Antifungal activities of spirolactone (**1**) in comparison with amphotericin B, itraconazole and voriconazole.

758

Strain number	Species	Section	amphotericin B MIC in mg/L	itraconazole MIC in mg/L	voriconazole MIC in mg/L	spirolactone MIC (MEC) in mg/L
SF011948	*Aspergillus brasiliensis*	Nigri	0.5	2	2	0.5 (0.25)
NRZ-2023-0685	*Aspergillus luchuensis*	Nigri	0.25	n.a.	1	0.5 (0.25)
NRZ-2021-0572	*Aspergillus citrinoterreus*	Terrei	4	0.5	0.5	0.5 (0.25)
SF013938	*Aspergillus neoafricanus*	Terrei	2	0.5	0.5	0.5 (0.25)
NRZ-2019-093	*Aspergillus terreus*	Terrei	8	0.5	1	0.125 (0.125)
NRZ-2019-116	*Aspergillus calidoustus*	Usti	16	8	4	0.5 (0.25)
SF006408	*Aspergillus ustus*	Usti	1	>8	>8	0.125 (0.06)
NRZ-2016-235	*Talaromyces marneffei*		0.06	≤0.016	≤0.016	0.125 (0.125)
NRZ-2021-0646	*Talaromyces purpureogenes*		1	>8	8	0.5 (0.25)

759 MIC: minimum inhibitory concentration.

760

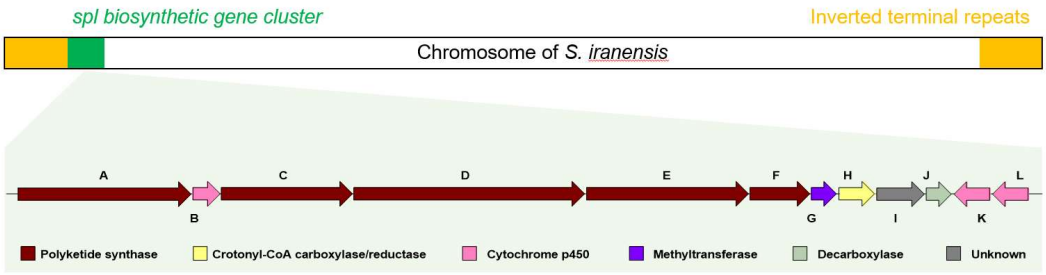

Fig. 1 Organization of the spirolactone biosynthetic gene cluster from *S. iranensis*. ORFs are shown as arrows indicating the size and direction of transcription.

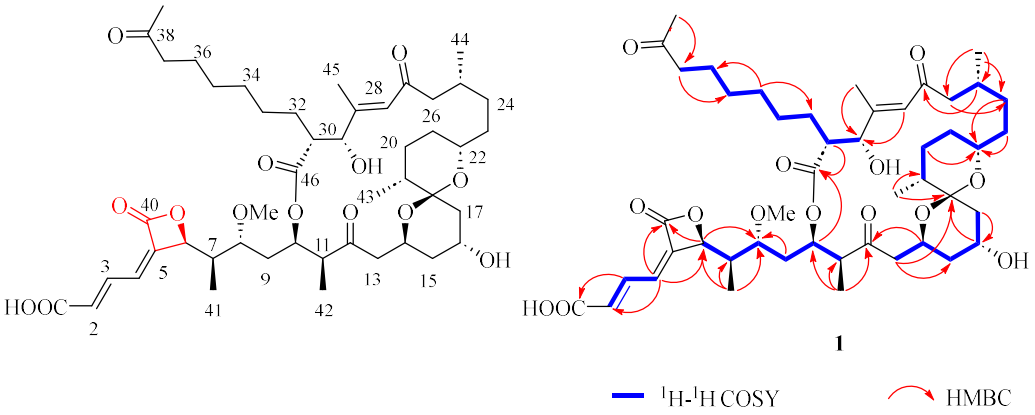

Fig. 2 Chemical structures of spirolactone (**1**) and selected ^{1}H-^{1}H COSY and HMBC correlations.

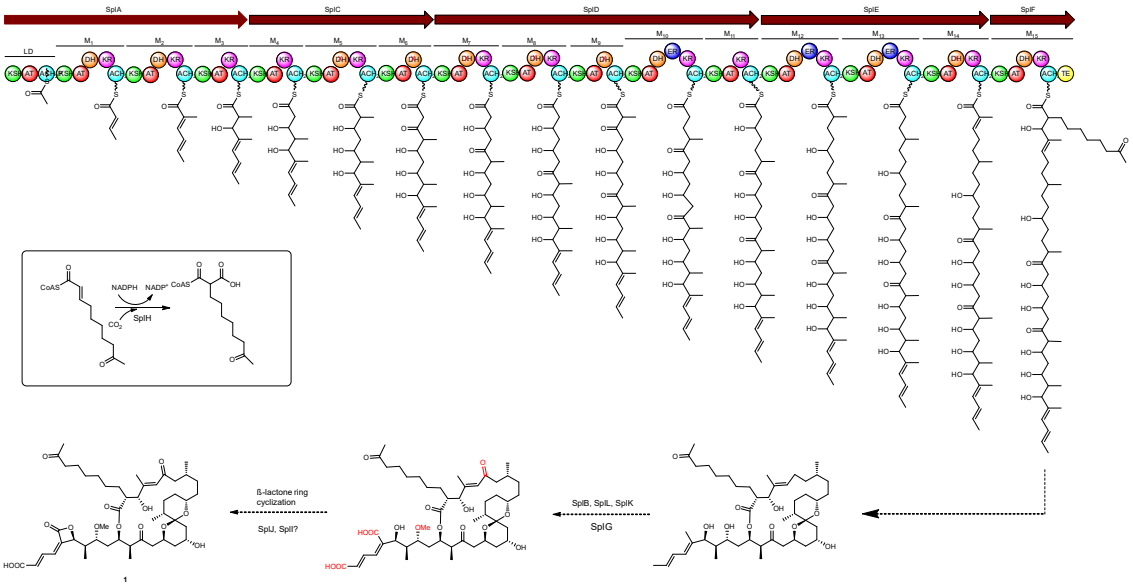

Fig. 3 Proposed biosynthesis pathway of spirolactone (**1**).

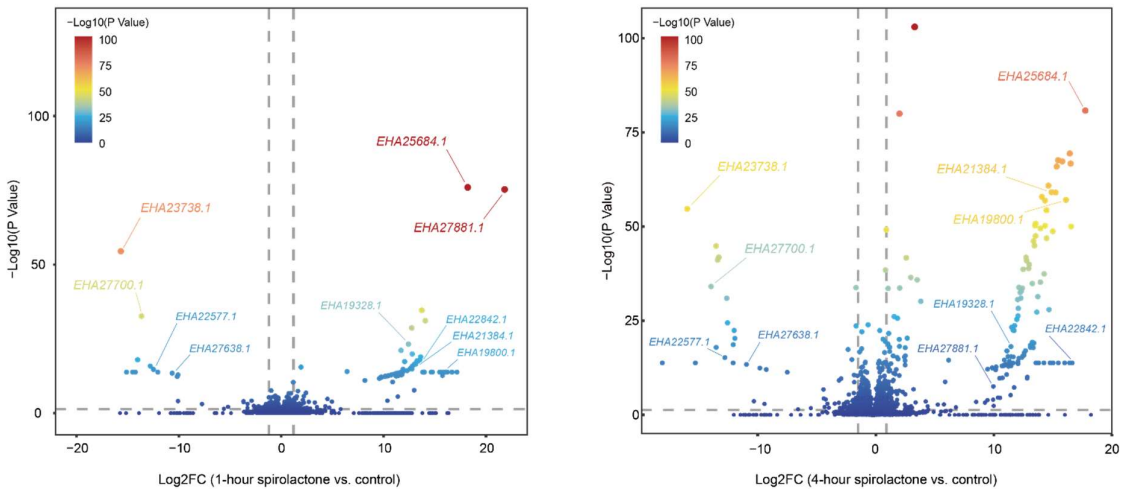

Fig. 4 Volcano plot of the abundance of protein after spirolactone treatment based on proteomics analysis.